

# A huge reservoir of ionized gas around the Milky Way: Accounting for the Missing Mass?

A. Gupta and S. Mathur

*Astronomy Department, Ohio State University, Columbus, OH 43210, USA*

agupta@astronomy.ohio-state.edu

Y. Krongold

*Instituto de Astronomia, Universidad Nacional Autonoma de Mexico, Mexico City,  
(Mexico)*

F. Nicastro

*Harvard-Smithsonian Center for Astrophysics, Cambridge, MA, 02138, USA*  
*Osservatorio Astronomico di Roma-INAF, Via di Frascati 33, 00040, Monte Porzio  
Catone, RM, (Italy)*

M. Galeazzi

*Physics Department, University of Miami, Coral Gables, FL 33124, USA*

## ABSTRACT

Most of the baryons from galaxies have been “missing” and several studies have attempted to map the circumgalactic medium (CGM) of galaxies in their quest. Recent studies with the Hubble Space Telescope have shown that many galaxies contain a large reservoir of ionized gas with temperatures of about  $10^5$  K. Here we report on X-ray observations made with the Chandra X-ray Observatory probing an even hotter phase of the CGM of our Milky Way at about  $10^6$  K. We show that this phase of the CGM is massive, extending over a large region around the Milky Way, with a radius of over 100 kpc. The mass content of this phase is over ten billion solar masses, many times more than that in cooler gas phases and comparable to the total baryonic mass in the disk of the Galaxy. The missing mass of the Galaxy appears to be in this warm-hot gas phase.

## 1. Introduction

We have known for a while that the baryonic mass of galaxies, including that of our own Milky way, falls short of what is expected for their total mass ((Sommer-Larsen 2006; Bregman 2007) and references therein). This “missing” mass is either ejected from galaxies into the intergalactic medium (IGM) or still resides in the circumgalactic medium (CGM). Our galaxy is a member of the Local Group of galaxies, and it is possible that the matter ejected from the Galaxy resides in the Local Group. Either in the CGM or in the Local Group medium (LGM), the baryonic mass is expected in a warm-hot gas phase at temperatures between  $10^5 - 10^7 K$ . This is probably the reason why earlier studies probing only cooler gas could not account for it. The warm component of this phase at  $10^5 - 10^6 K$  has been observed in the UV traced by absorption lines of ionized metals, in particular O VI (Nicastro et al. 2003; Sembach et al. 2003). Recent observations with the Hubble Space Telescope (HST) have shown that the CGM around star-forming galaxies is large (150 kpc) and the mass of the warm phase traced by O VI exceeds that of the gas in the galaxies themselves (Tumlinson et al. 2011; Tripp et al. 2011). Using other absorption lines, e.g. Si IV and C IV in the UV (Lehner & Howk 2011) found that there is a large reservoir of warm ionized gas around our Galaxy as well.

The hotter phase of the warm-hot gas, at temperatures  $10^6 - 10^7 K$  can be probed by even more highly ionized metals. The dominant transitions from such ions lie in the soft-X-ray band and indeed, absorption lines due to O VII and O VIII at redshift zero have been detected toward extragalactic sight-lines by the Chandra X-ray Observatory and the XMM-Newton Observatory (Nicastro et al. 2005; Williams et al. 2005; Williams et al. 2007). The distribution, spacial extent, and mass of the warm-hot gas provide important constraints to the models of large scale structure formations (e.g., (Cen & Ostriker 1999)) and/or outflows/inflows from galaxies (e.g. (Stinson et al. 2011)), but these parameters are difficult to measure in part due to the limited spectral resolution of *Chandra* and *XMM-Newton* and in part because of the inherent difficulty in using the absorption line studies alone. Here we use both absorption and emission observations to derive the physical properties of the warm-hot plasma. We show that the X-ray observations probe million degree gas, with low density, extending over 100 kpc and having mass over ten billion solar masses. This is several times more than previously found in the CGM of the Milky Way. Alternatively, the warm-hot gas we probe is from the extended LG medium.

## 2. Sample selection & Data reduction

We search for and measure the absorption lines from highly ionized gas at  $z \sim 0$ , as seen in the spectra of most of the extragalactic sight-lines toward bright active galactic nuclei (AGNs). We use high signal-to-noise ratio observations with *Chandra* High Energy Transmission Grating (HETG) or Low Energy Transmission Grating (LETG) with focus on O VII and O VIII absorption lines at  $\lambda = 21.602 \text{ \AA}$  and  $\lambda = 18.967 \text{ \AA}$  respectively.

We began by selecting all the *Chandra* grating observations of AGNs that were publicly available as of 2011 October 30 and that had exposure time of at least 100 *ks*. This resulted in multiple observations of 50 targets with both grating spectrometers aboard *Chandra* (HETG and LETG).

We reduced the data using the standard *Chandra* Interactive Analysis of Observations (CIAO) software (v4.3) and *Chandra* Calibration Database (CALDB, v4.4.2) and followed the standard *Chandra* data reduction threads. For the *Chandra* ACIS/HETG and ACIS/LETG observations, we co-added the negative and positive first-order spectra and built the effective area files (ARFs) for each observations using the *fullgarf* CIAO script. Those pertaining to the ACIS/LETG observations were corrected for the ACIS quantum efficiency degradation. Unlike ACIS, the HRC does not have the energy resolution to sort individual orders, and each spectrum contains contributions from all the diffraction orders. For the HRC/LETG observations we used the standard ARF files for orders 1 through 6 and convolved it with the relevant standard redistribution matrix file (RMF). For the targets with multiple observations, we added the grating spectra and averaged the associated ARFs using the *ciao* script *add\_grating\_spectra*, to increase the signal to noise ratio of the spectra. We only add the observations with the same instrumental configuration and the observations made with different instruments are analyzed separately.

Of the 50 sight lines initially selected, 29 have good enough signal-to-noise ratios (S/N) near  $21.6 \text{ \AA}$  to detect O VII absorption lines. The strong O VII  $K\alpha$  absorption lines near  $21.602 \text{ \AA}$  are clearly visible in 21 out of 29 sources with good signal-to-noise spectra; thus the covering fraction of the O VII systems is  $21/29 = 0.72$ . In 30% of the sources significant O VIII  $K\alpha$  lines near  $18.967 \text{ \AA}$  are also observed. Here we consider a sub-sample of 8 targets (Table 1), where both O VII and O VIII  $K\alpha$  local absorption has been confidently detected (we have not included 3C273 in this sample of 29 sources because the  $z = 0$  absorption lines in this sight-line might be from a nearby supernova remnant). The detailed analysis of the complete sample will be presented in a forthcoming paper (Gupta et al. 2012, in preparation). The local ( $z \sim 0$ ) O VII and O VIII absorption lines in 3 of our 8 targets have been reported previously by other authors, but to ensure the consistency of data analysis, we reanalyzed all the data and obtained the fit results independently; for the other five targets

we present new detections of  $z \sim 0$  lines.

### 3. Analysis

#### 3.1. Continuum, Intrinsic Absorption, and Emission

The HETG and LETG spectra are binned to  $0.01 \text{ \AA}$  and  $0.025 \text{ \AA}$  respectively and analyzed using the CIAO fitting package *Sherpa*. Since we are interested in oxygen absorption lines we fit the spectral continuum in the  $17 - 23 \text{ \AA}$  range with a simple power law and a Galactic absorbing column density ( $N_H$ , from (Dickey et al. 1990)). For the targets Mrk290 and NGC3783 we need to add a black-body component to account for the soft excess, that could come from a standard optically-thick accretion disk. In our sample, the photon index of the power-law varies from  $1.4 - 2.1$  with average value of 2.0.

Our targets are nearby Type 1 AGNs, which have their own intrinsic absorption and emission features. We carefully study all the spectra to confirm that none of the AGN intrinsic features contaminates the local ( $z = 0$ ) absorption lines. Except for one source, NGC4051, the intrinsic lines are sufficiently red-shifted that they do not contaminate the local O VII and O VIII absorption lines. For this reason we do not include NGC4051 in our final sample. We then modeled all the statistically significant AGN intrinsic absorption and emission features with Gaussian components.

#### 3.2. Local ( $z \sim 0$ ) Absorption

After fitting the continuum and intrinsic features as described above, the local O VII and O VIII  $K\alpha$  absorption lines are detected with  $\geq 3\sigma$  and  $\geq 2\sigma$  significance levels respectively. In 6 sources, we also detected the O VII  $K\beta$  absorption line near  $18.62\text{\AA}$ . We fit these lines in *Sherpa* with narrow Gaussian features. Since with Chandra gratings ( $FWHM = 0.05 \text{ \AA}$  for LEG and  $FWHM = 0.023 \text{ \AA}$  for MEG) the lines are unresolved, we fix the line width to  $1 m\text{\AA}$ . Errors are calculated using the *projection* command in *Sherpa*, allowing the overall continuum normalization to vary along with all parameters for each line. For the observations with no detection of O VII  $K\beta$ , we fixed the line centroid at  $18.629 \text{ \AA}$  and obtained the upper limits on equivalent widths (EW). The best-fit line equivalent widths (EWs) and statistical uncertainties are given in Table 2 and the spectra are shown in figure 1.

### 3.3. Column Density Measurement

For optically thin gas the ionic column density depends simply on the observed equivalent width:  $N(ion) = 1.3 \times 10^{20} (\frac{EW}{f\lambda^2})$ , where  $N(ion)$  is the ionic column density ( $cm^{-2}$ ),  $EW$  is the equivalent width ( $\text{\AA}$ ),  $f$  is the oscillator strength of the transition, and  $\lambda$  is in  $\text{\AA}$ . However, at the measured column densities of N(O VII), saturation could be an important issue as suggested by simulations (Chen et al. 2003) and observational studies of Mrk421 (Williams et al. 2005). Therefore to correctly convert the measured equivalent widths to ionic column densities, we require knowledge of the Doppler parameter  $b$ ; at a fixed EW, column density decreases with increasing  $b$ . The low velocity resolution of *Chandra* gratings makes it unfeasible to directly measure the O VII line width. If multiple absorption lines from the same ion are detected, the relative equivalent widths of these lines can instead be used to place limits on the column density N(O VII) and the Doppler parameter  $b$  of the medium.

To use this technique, we searched for and detected O VII  $K\beta$  line at 18.629  $\text{\AA}$  in 6 out of 8 targets and measured the upper limit for the remaining two. For O VII, the expected  $\frac{EW(K\beta)}{EW(K\alpha)}$  ratio is  $\frac{f(K\beta) \times \lambda^2(K\beta)}{f(K\alpha) \times \lambda^2(K\alpha)} = 0.156$ . Our observations indicate that most O VII  $K\alpha$  lines are saturated (Table 2). To place quantitative constraints on N(O VII) and the  $b$  parameter we employ the technique described in details in (Williams et al. 2005). For a given absorption line with a measured equivalent width and known oscillator strength  $f$  value, the inferred column density as a function of the  $b$  parameter can be calculated using the relations from (Spitzer 1978). The  $b$  and N(O VII) can be determined for a range of Doppler parameters for which both  $K\alpha$  and  $K\beta$  transitions provide consistent N(O VII) measurements. Figure 2 shows such  $1\sigma$  contours for the measured O VII  $K\alpha$  and  $K\beta$  transitions for NGC3783. As the figure show, the  $1\sigma$  constraints on Doppler parameter  $b$  and O VII column densities are  $45 < b < 128 \text{ km s}^{-1}$  and  $16.03 < \log N(\text{O VII}) < 16.68 \text{ cm}^{-2}$ , respectively. For Mrk421 and PKS2155-304 we used the  $b$  parameter values from (Williams et al. 2005; Williams et al. 2007). Following the same method, we constrained the  $b$  parameter and O VII column densities for all other observations. The O VII column densities range from  $\log N(\text{O VII}) = 15.82$  to  $16.50 \text{ cm}^{-2}$ , with a weighted mean value of  $\log N(\text{O VII}) = 16.19 \pm 0.08 \text{ cm}^{-2}$ . These values of N(O VII) are higher than measured by other authors (Fang et al. 2006; Bregman et al. 2007) who assumed the lines to be unsaturated.

#### 4. Results

Column density ratios of different ions of the same element depend on the physical state of the medium and provide the rigorous constraints on the temperature of the absorbing medium. Given that we detect both O VII and O VIII, we place a tight constraint on the temperature  $\log T = 6.1 - 6.4 K$ , assuming the gas to be in collisional ionization equilibrium.

With the spectral resolution of current X-ray gratings it is difficult to resolve the absorption lines into Galactic and Local Group components. However a comparison between emission and absorption measurements, provides us with a great tool to analyze the properties of the X-ray absorbers. The absorption lines measure the column density of gas  $N_H = \mu n_e R$ , where  $\mu$  is the mean molecular weight  $\approx 0.8$ ,  $n_e$  is the electron density and  $R$  is the path-length. The emission measure, on the other hand, is sensitive to the square of the number density of the gas ( $EM = n_e^2 R$ , assuming a constant density plasma). Therefore a combination of absorption and emission measurements naturally provides constraints on the density and the path-length of the absorbing/emitting plasma.

(Henley et al. 2010) and (Yoshino et al. 2009) using *XMM-Newton* and *Suzaku* data respectively, found that the Galactic halo temperature is fairly constant across the sky ( $1.8 - 2.4 \times 10^6 K$ ), but the halo emission measure varies by an order of magnitude ( $0.0005 - 0.005 \text{ cm}^{-6} \text{ pc}$ ) with an average of  $EM = 0.0030 \pm 0.0006 \text{ cm}^{-6} \text{ pc}$ , assuming solar metallicity. Other measurements of Galactic Halo emission (McCammon et al. 2002; Galeazzi et al. 2007; Gupta et al. 2009; Hagihara et al. 2010) also reported  $EM \sim 0.003 \text{ cm}^{-6} \text{ pc}$  for solar metallicity, close to the average. Thus using  $EM = 0.003 (\frac{Z}{Z_\odot}) \text{ cm}^{-6} \text{ pc}$ , we solve for the path length and electron density of the absorbing gas. Combining absorption and emission the density is:

$$n_e = (2.0 \pm 0.6 \times 10^{-4}) \left( \frac{0.5}{f_{OVII}} \right)^{-1} \text{ cm}^{-3} \quad (1)$$

and the path length:

$$R = 71.8 \pm 30.2 \left( \frac{8.51 \times 10^{-4}}{(A_O/A_H)} \right) \left( \frac{0.5}{f_{OVII}} \right)^2 \left( \frac{Z_\odot}{Z} \right) \text{ kpc} \quad (2)$$

where the Solar Oxygen abundance of  $A_O/A_H = 8.51 \times 10^{-4}$  is from (Anders & Grevesse 1989),  $f_{OVII}$  is the ionization fraction of O VII and  $Z$  is the metallicity. For the observed temperature of about  $\gtrsim 10^6 K$ , it is reasonable to expect  $f = 0.5$  (see, e.g., figure 4 in (Mathur et al. 2003)). Cosmological simulations (Toft et al. 2002; Sommer-Larsen 2006) of formation and evolution of disc galaxies show that outside the galactic disk the mean metallicity of gas is

$Z = 0.2 \pm 0.1 Z_{\odot}$ . These values of metallicities are also consistent with observational results for the outskirts of groups (Rasmussen et al. 2009) and clusters of galaxies (e.g., (Tamura et al. 2004)). Thus it is highly unlikely that in the CGM metallicity is as high as  $Z_{\odot}$ . Newer values of oxygen abundance are even lower (Holweger 2001; Asplund et al. 2009); making  $L$  larger. We therefore use  $Z = Z_{\odot}$  to set an upper limit on the pathlength and a lower limit on the electron density. The  $1\sigma$  limits on the pathlength and density are  $L > 41.6$  kpc and  $n_e < 2.6 \times 10^{-4} \text{ cm}^{-3}$

Using this lower limit on the pathlength and the observed O VII column density we can also estimate the total baryonic mass traced by the O VII absorbers, assuming a homogeneous spherically symmetric system:

$$M_{total} > 1.7 \times 10^9 \left(\frac{f_c}{0.72}\right) \left(\frac{8.51 \times 10^{-4}}{(A_O/A_H)}\right)^3 \left(\frac{Z_{\odot}}{Z}\right)^3 \left(\frac{0.5}{f_{OVII}}\right)^5 M_{\odot} \quad (3)$$

where  $f_c$  is the covering factor,  $\sim 72\%$  for our entire sample.

For the Solar abundance used by (Tumlinson et al. 2011)  $M_{total} = 1.2 \times 10^{10} M_{\odot}$ , compared to  $2 \times 10^9 M_{\odot}$  found by (Tumlinson et al. 2011) in O VI systems. For  $Z = 0.3Z_{\odot}$ , which is far more likely, the path-length becomes as large as  $L > 138$  kpc and the mass  $M_{total} > 6.1 \times 10^{10} M_{\odot}$ . Thus we find that the O VII / O VIII systems probe the reservoir of gas in the CGM extending to over 100 kpc. The mass probed by this warm-hot gas is larger than that in any other phase of the CGM and is comparable to the entire baryonic mass of the Galactic disk  $\sim 6 \times 10^{10} M_{\odot}$  (Sommer-Larsen 2006).

#### 4.1. Assumptions and Biases

We have combined our measurements of the O VII and O VIII column densities with the published values of emission measure (EM) to derive physical conditions in the absorbing/emitting plasma, viz. temperature, density, path-length and mass. The constraint on the temperature is robust; it depends simply on the O VII to O VIII column density ratio, under the assumption of collisional ionization equilibrium. For our measured density of a few times  $10^{-4} \text{ cm}^{-3}$ , which is several thousand times larger than the mean density of the Universe ( $n = 1.88 \times 10^{-7} \text{ cm}^{-3}$ ), photoionization becomes unimportant and collisional ionization is a reasonable assumption.

We have assumed that the absorbing/emitting plasma is of uniform density; this need not be the case. The distribution of warm-hot gas around several galaxies follows a beta-model profile in which the density is high in the center and falls off with radius (see

(Mathur et al. 2008) and references therein); gas in clusters and groups of galaxies also follows similar profile. In any case, if the gas is not of uniform density, the EW would be weighted by the denser gas and for the same observed column density the average density would be smaller and the inferred path-length would be larger extending into the LG medium. We cannot rule out the possibility that the warm-hot gas we trace is from the LG medium instead.

As noted above, our sample is made of sight-lines in which both O VII and O VIII  $K\alpha$  absorption lines at  $z = 0$  are securely detected. Does this mean that our sample is biased toward high column density systems? If so, the path-length and the mass of the warm-hot plasma could be severely over-estimated. In figure 4 we have plotted the EW distribution of O VII line in all 29 sources in the parent sample. The sub-sample of 8 sources is marked by the red shaded region; it is clear that this sub-sample is *not* biased toward high EW systems. The high EW systems are not in the sub-sample of this paper because they do not have clean detections of O VIII lines, in large part because of the contamination from intrinsic absorption. It is also worth noting that the upper limits on the EWs in targets with non-detections of O VII  $K\alpha$  line is higher than the average of the parent sample in all but one cases. All together, we argue that the average EW of our sub-sample is a fair representation of the large sample and that our sample is *not* biased toward high column density systems.

## 5. Conclusions

For reasonable values of parameters and with reasonable assumptions, the *Chandra* observations of O VII and O VIII absorption lines at  $z = 0$  imply that there is a huge reservoir of ionized gas around the Milky Way. It may be in the halo of the Milky Way or in the surrounding Local Group. Either way, its mass appears to be very large.

## REFERENCES

- Anders, E. & Grevesse, N., *Geochimica et Cosmochimica Acta*, **53**, 197A
- Asplund, M., Grevesse, N., Sauval, A.J., & Scott, P. 2009, *Ann. Rev. Astron. Astro.*, **47**, 481
- Bregman, J.N. 2007, *Ann. Rev. Astron. Astro.*, **45**, 221
- Bregman, J.N., & Lloyd-Davies, E.J. 2007, *Astrophys. J.*, **669**, 990
- Cen, R., & Ostriker, J. P. 1999, *Astrophys. J.*, **514**, 1



- Chen, X., Weinberg, D.H., Katz, N., & Davè, R. 2003, *Astrophys. J.*, **594**, 42
- Dickey, J.M., & Lockman, F.J. 1990, *Ann. Rev. Astron. Astro.*, **28**, 215
- Fang, T.T., Canizares, C.R., & Wolfire, M. 2006, *Astrophys. J.*, **644**, 174
- Galeazzi, M., Gupta, A., Covey, K., & Ursino, E. 2007, *Astrophys. J.*, **658**, 1081
- Gupta, A. et al. 2012, *in preparation*
- Gupta, A. et al. 2009, *Astrophys. J.*, **707**, 644
- Hagihara, T. et al. 2010, *Publication of the Astronomical Society of Japan*, **62**, 723
- Henley, D.B. et al. 2010, *Astrophys. J.*, **723**, 935
- Holweger, H. *AIPC*, **598**, 23H
- Lehner, N., & Howk, J.C. 2011, *Science*, **334**, 955
- Mathur, S., Weinberg, D.H., & Chen, X. 2003, *Astrophys. J.*, **582**, 82
- Mathur, S., Sivakoff, G.R., Williams, R.J., & Nicastro, F. 2008, *Astrophys. J.*, **315**, 93
- McCammon, D., et al. 2002, *Astrophys. J.*, **576**, 188
- Nicastro, F., Zezas, A., Elvis, M., Mathur, S., Fiore, F., CecchiPestellini, C., Burke, D., Drake, J., & Casella, P. et al. 2003, *nature*, **421**, 719
- Nicastro, F., et al. 2005, *nature*, **433**, 49
- Rasmussen, J., & Pedersen, K., 2001, *Astrophys. J.*, **559**, 892
- Rasmussen, A., Kahn, S.M., & Paerels, F. 2003, *ASSL Vol. 281: The IGM/Galaxy Connection. The Distribution of Baryons at z=0*, 109
- Rasmussen, A., et al. 2009, *Astrophys. J. Suppl. Ser.*, **697**, 79
- Savage, B.D., et al. 2003, *Astrophys. J.*, **146**, 125
- Savage, B.D., Wakker, B.P., Fox, A. J., & Sembach, K.R. 2005, *Astrophys. J.*, **619**, 863
- Sembach, K.R., et al. 2003, *Astrophys. J. Suppl. Ser.*, **146**, 165
- Spitzer, L. 1978, *Physical Processes in the Interstellar Medium*, John Wiley & Sons 1978, 336

- Sommer-Larsen, J. 2006, *Astrophys. J.*, **644**, L1
- Stinson, G. et al. 2011, arXiv:1112.1698
- Tamura, T. et al. 2004, *A&A*, **420**, 135
- Toft, S., Rasmussen, J., Sommer-Larsen, J., & Pedersen, K. et al. 2002, *MNRAS*, **335**, 799
- Tumlinson, J. et al. 2011, *Science*, **334**, 948
- Tripp, T.M. et al. 2011, *Science*, **334**, 952
- Williams, R.J. et al. 2005, *Astrophys. J.*, **631**, 856
- Williams, R.J., Mathur, S., Nicastro, F., & Elvis, M., 2007, *Astrophys. J.*, **665**, 247
- Yoshino, T. et al. 2009, *Publication of the Astronomical Society of Japan*, **61**, 805

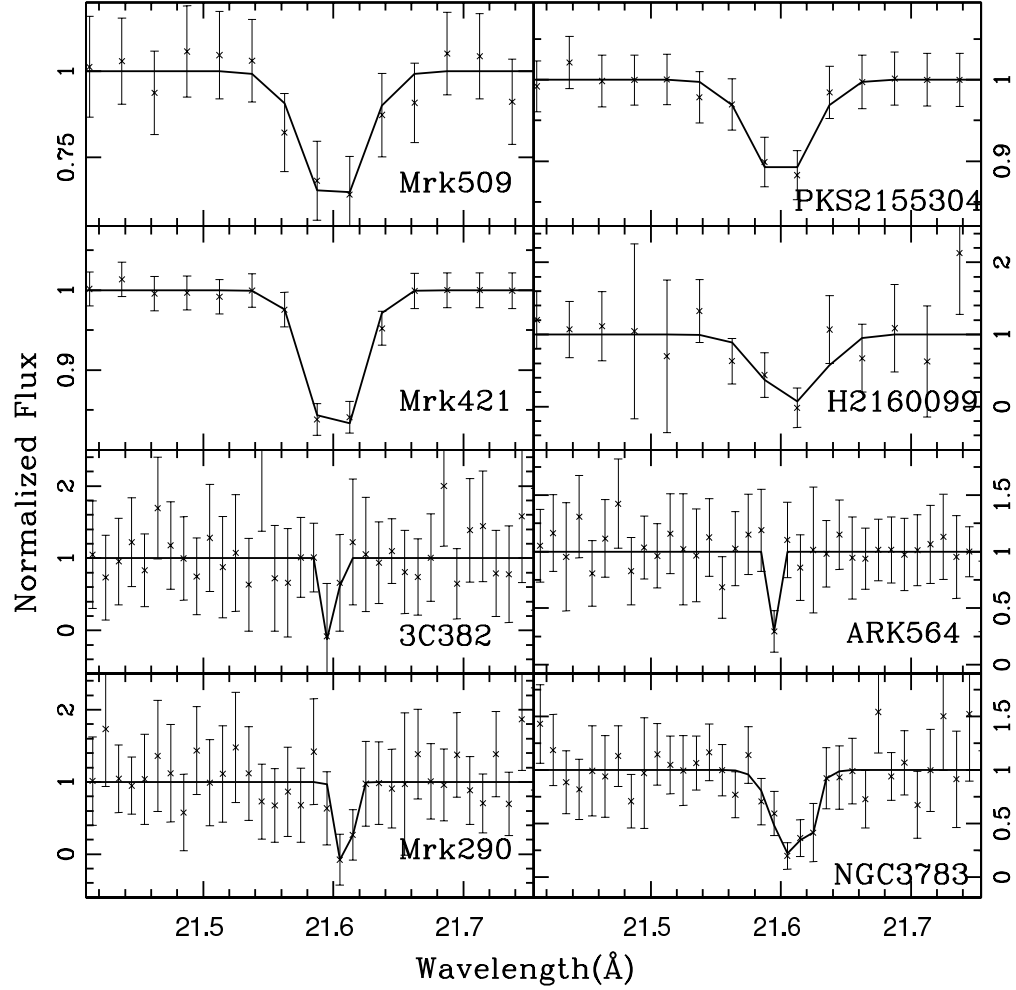


Fig. 1.— The normalized flux at the location of the O VII line at 21.602 Å.

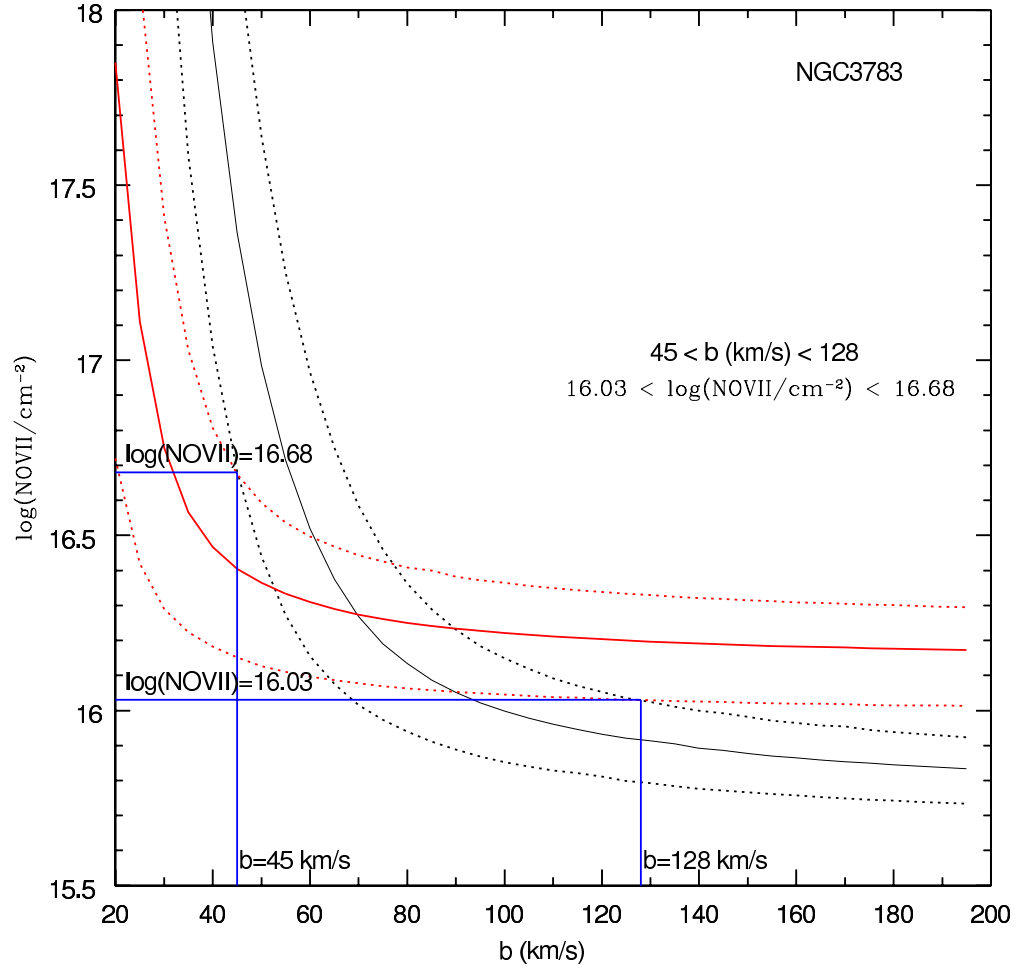


Fig. 2.— Contours of allowed column densities  $N(\text{O VII})$  and Doppler parameters  $b$  for the  $\text{O VII}_{K\alpha}$  (black) and  $\text{O VII}_{K\beta}$  (red).

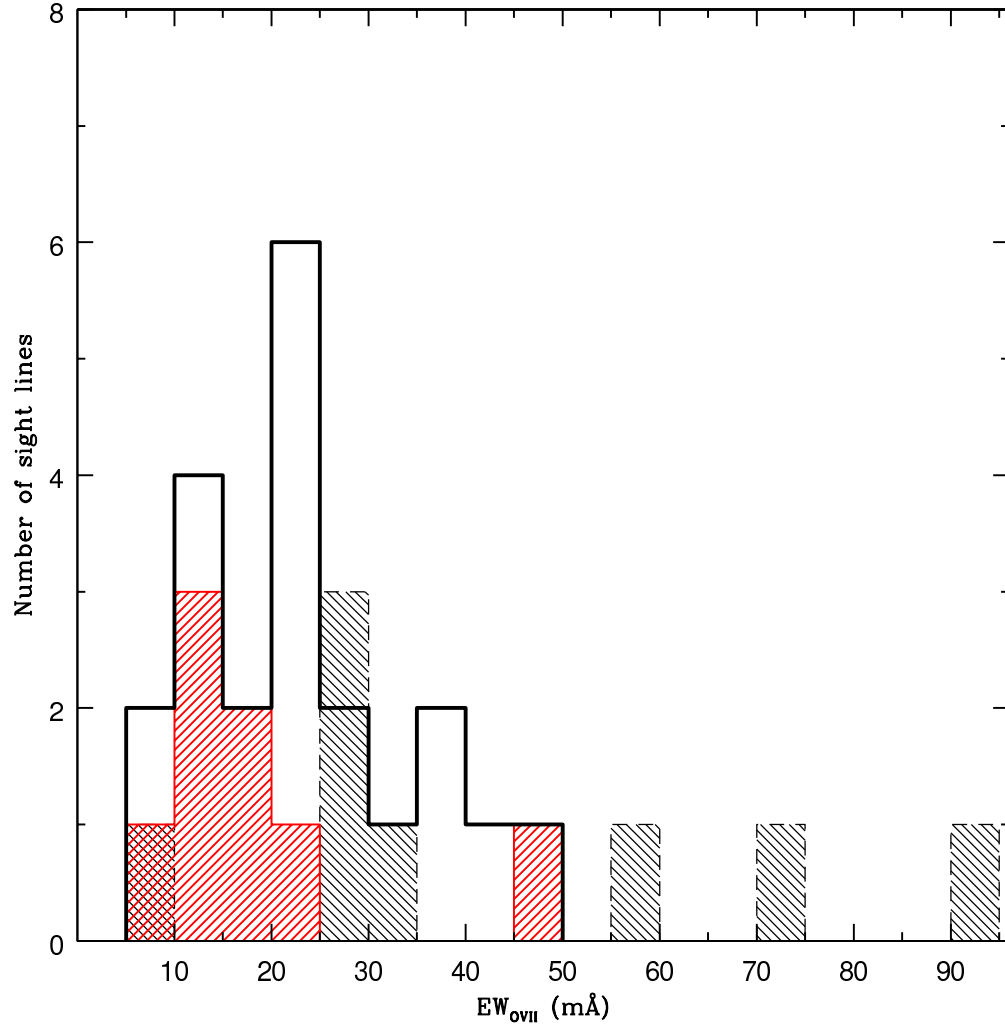


Fig. 3.— Distribution of O VII  $\kappa\alpha$  line EW for the parent sample. The solid black line corresponds to distribution for the 21 observations in which O VII  $\kappa\alpha$  lines are clearly visible. The black shaded region marked the  $1\sigma$  upper limits on the O VII  $\kappa\alpha$  EW for 8 observations with no (or less than  $1\sigma$  significance) detection. The red shaded region corresponds to sub-sample selected for this study (see text).

Table 1: Summary of the targets used in this investigation.

Target	l	b	Redshift	Exposure
	<i>deg</i>	<i>(deg)</i>	<i>z</i>	<i>(ks)</i>
Mrk290	91.48	47.95	0.0304	250
PKS2155-304	17.73	-52.24	0.1160	530
Mrk421	179.83	65.03	0.0300	720
Mrk509	35.97	-29.86	0.0344	460
3C382	61.30	17.44	0.0579	120
Ark564	92.13	-25.33	0.0247	250
NGC3783	287.45	22.94	0.0097	905
H2106-099	40.26	-34.93	0.0265	100

Table 2: The O VII and O VIII absorption line measurement.

Target	EW (O VII $K\alpha$ ) ( $m\text{\AA}$ )	EW (O VII $K\beta$ ) ( $m\text{\AA}$ )	EW (O VIII $K\alpha$ ) ( $m\text{\AA}$ )	O VII ( $\frac{EW(K\beta)}{EW(K\alpha)}$ )	$b$ $km/s$	$\log(N_{O VII})$ $cm^{-2}$
Mrk290	$18.9 \pm 4.5$	$5.1 \pm 3.7$	$8.4 \pm 2.9$	$0.27 \pm 0.21$	$> 55$	$16.14 \pm 0.32^*$
PKS2155-304	$11.6 \pm 1.6$	$4.2 \pm 1.3$	$6.7 \pm 1.4$	$0.36 \pm 0.12$	35 – 94	$16.09 \pm 0.19$
Mrk421	$9.4 \pm 1.1$	$4.6 \pm 0.7$	$1.8 \pm 0.9$	$0.49 \pm 0.09$	24 – 55	$16.22 \pm 0.23$
Mrk509	$23.9 \pm 5.0$	$11.7 \pm 4.1$	$10.3 \pm 4.3$	$0.49 \pm 0.20$	70 – 200	$16.7 \pm 0.27$
3C382	$17.3 \pm 5.0$	$7.8 \pm 3.0$	$6.8 \pm 3.8$	$0.45 \pm 0.22$	$> 40$	$16.50 \pm 0.49^*$
Ark564	$12.0 \pm 1.9$	$< 3.8$	$9.5 \pm 4.1$	...	$> 20$	$15.82 \pm 0.20^*$
NGC3783	$14.4 \pm 2.5$	$5.6 \pm 1.6$	$4.5 \pm 2.9$	$0.39 \pm 0.13$	50 – 130	$16.30 \pm 0.25$
H2106-099	$48.3 \pm 18.0$	$< 34.2$	$28.8 \pm 13.8$	...	$> 70$	$16.23 \pm 0.16^*$

\*The lower limit on O VII column densities are calculated using the curve-of-growth analysis.